Neural Networks 27 (2012) 32–37

Contents lists available at SciVerse ScienceDirect

Neural Networks

journal homepage: www.elsevier.com/locate/neunet

Asynchronous frameless event-based optical flow

Ryad Benosman [a,*], Sio-Hoi Ieng [a], Charles Clercq [b], Chiara Bartolozzi [b], Mandyam Srinivasan [c]

[a] Vision Institute, University Pierre and Marie Curie-UPMC/CNRS UMR7222, Paris, France

[b] Italian Institute of Technology, Genova, Italy

[c] University of Queensland at the Queensland Brain Institute, Australia

ARTICLE INFO

Article history:
Received 9 July 2011
Received in revised form 3 October 2011
Accepted 2 November 2011

Keywords:
Asynchronous acquisition
Spikes
Temporal dynamics
Event-based vision
Frameless vision
Optical flow

ABSTRACT

This paper introduces a process to compute optical flow using an asynchronous event-based retina at high speed and low computational load. A new generation of artificial vision sensors has now started to rely on biologically inspired designs for light acquisition. Biological retinas, and their artificial counterparts, are totally asynchronous and data driven and rely on a paradigm of light acquisition radically different from most of the currently used frame-grabber technologies. This paper introduces a framework for processing visual data using asynchronous event-based acquisition, providing a method for the evaluation of optical flow. The paper shows that current limitations of optical flow computation can be overcome by using event-based visual acquisition, where high data sparseness and high temporal resolution permit the computation of optical flow with micro-second accuracy and at very low computational cost.

1. Introduction

Asynchronous event-based artificial retinas are beginning to provide a paradigm shift in the current approaches to tackling visual signal processing (Lichtsteiner, Posch, & Delbruck, 2008; Posch, 2010). Conventional, frame-based image acquisition and processing technologies are not computationally efficient because they are not designed to take full advantage of the dynamic characteristics of visual scenes. Event-based dynamic vision sensors, on the other hand, provide a novel and efficient way for encoding light and its temporal variations by registering and transmitting only the changes at the exact time at which they occur (Lenero-Bardallo, Serrano-Gotarredona, & Linares-Barranco, 2011; Lichtsteiner et al., 2008; Posch, Matolin, & Wohlgenannt, 2011). As we shall show in this paper, the technique of event-based light encoding enables us to derive an event-based methodology for the computation of optical flow at high speed and at a very low computational cost.

There is no notion of frames in biological visual systems: the retina's outputs are massively parallel, asynchronous and data-driven. Neurons fire in an unsynchronized manner according to the information retrieved in scenes (Roska, Alyosha, & Werblin, 2006). Event-based retinas sense and encode the spatial locations (addresses) and times of changes in light intensity at the pixel level (Boahen, 2005). The resulting data is sparse and asynchronous. Unlike the situation in frame-based imaging, event-based pixels handle their own information and provide their location in the array, and a predefined indication of light change (Lichtsteiner et al., 2008). The notion of a general synchronous time applied to a set of pixels is replaced by a spatio-temporal record of events in which space and time are the encoded parameters. Consequently, event-based retinas' pixels have a very high temporal resolution of the order of thousand to tens of thousands of frames per second, thus exceeding the speed of most conventional frame based cameras by many orders of magnitude.

Optical flow computation is crucial for navigation, obstacle avoidance, distance regulation, and tracking moving targets. An efficient implementation is particularly important for mobile robots with limited power and tight payload constraints.

Optical flow estimation has been intensively studied for over two decades. State-of-the-art methods allow a robust calculation for a variety of applications, but are still far from being fully satisfactory, as the estimation of dense flow fields for fast motions in real world environments cannot be achieved reliably. Existing optical flow techniques originate from two main concepts: the energy minimization framework proposed by Horn and Schunck (1980), and the coarse-to-fine image warping introduced by Lucas and Kanade (1981a) to handle large displacements. These ideas have been extended by using statistical techniques to lower the impact of outliers to yield reliable results even in situations that involve occlusions or motion discontinuities (Black & Anandan, 1996; Memin & Perez, 1998). Some techniques are even robust to illumination changes by introducing gradient consistency (Brox, Bruhn, Papenberg, & Weickert, 2004), with the constraint of small displacements.

* Corresponding author.
E-mail addresses: ryad.benosman@upmc.fr (R. Benosman), sio-hoi.ieng@upmc.fr (S.-H. Ieng), charles.clercq@iit.it (C. Clercq), chiara.bartolozzi@iit.it (C. Bartolozzi), M.Srinivasan@uq.edu.au (M. Srinivasan).

0893-6080/$ – see front matter © 2011 Elsevier Ltd. All rights reserved.
doi:10.1016/j.neunet.2011.11.001

In order to tackle large displacements, some methods rely on multi-scales techniques. The flow is computed from coarse-to-fine scales, allowing the coarser scales to provide an initialization of the global computation. However, these downscaling techniques perform spatial smoothing, which means that the computed flow is dominated by the motion of large structures and does not accurately estimate the motion of small structures undergoing large motions (Fransens, Strecha, & Gool, 2007).

Techniques based on the matching of sparse descriptors are robust to large displacements at the cost of lower accuracy. The main advantage of such techniques is to provide a reliable initial match, taking into account small scale structures missed by the coarse-to-fine optical flow. The initial set of sparse hypotheses is then integrated into variational approaches to guide local optimizations taking into account large displacements (Alexander, Arteaga, David, & Tomas, 2008; Amiaz, Lubetzky, & Kiryati, 2007; Brox et al., 2004). Variational optimizations provide dense estimates with subpixel accuracy, estimates making use of geometric constraints and all available image information (Liu, Hong, Herman, Camus, & Chellappa, 1998). Their main drawback is the influence of outliers and the dependence on the choice of the initialization scale. The high computational cost of the all of the approaches described above requires power hungry and time consuming software implementations, which are not adapted for real-time applications such as mobile autonomous robotics. The frame-based optical flow's computations remain linked to the frequency of the camera used, they usually do not exceed 60 Hz.

2. Neuromorphic silicon retina

2.1. State of the art

In the late 1980s, it was shown (Mead, 1989) that standard semiconductor technology can be used for implementing circuits that mimic neural functions and realize building blocks that emulate the operation of their biological models, i.e. neurons, axons, synapses, photoreceptors, etc., thus enabling the construction of biomimetic artifacts that combine the assets of silicon VLSI technology with the processing paradigms of biology. The notion that binds work on such neuromorphic systems is a desire to emulate Nature's use of asynchronous, exceedingly sparse, data-driven digital signaling as a core aspect of its computational architecture. Neuromorphic systems, as the biological systems they model, process information using energy-efficient, often massively parallel, event-driven methods. Since the seminal implementation of a "silicon retina" by Mahowald and Mead (1991) in 1989, a variety of biomimetic vision devices has been developed (Boahen, 2005; Lichtsteiner et al., 2008). Neuromorphic vision sensors feature massively parallel pre-processing of the visual information at the pixel level, combined with highly efficient asynchronous, event-based information encoding and data communication. Event-based sensors allow a radical new variety of processing (Braddick, 2001; Chicca, Lichtsteiner, Delbruck, Indiveri, & Douglas, 2006; Choi, Merolla, Arthur, Boahen, & Shi, 2005; Serrano-Gotarredona et al., 2009; Serrano-Gotarredona, Serrano-Gotarredona, Acosta-Jimenez, & Linares-Barranco, 2006).

2.2. The visual input events

The neuromorphic vision sensors built from the pioneering work are also called Dynamic Vision Sensors (DVSs). The DVS models the transient responses of the retina (Roska et al., 2006). The stream of events from the retina can be defined mathematically as follows: let $e(\mathbf{p}, t)$ be an event occurring at time t at the spatial location $\mathbf{p} = (x, y)^T$. The values $e(\mathbf{p}, t)$ are set to be -1 or $+1$ when a negative or a positive change of contrast is detected respectively. The absence of events when no change of contrast is detected implies that redundant visual information usually recorded in frames are not carried in the stream of events. Fig. 1 shows an example of the spatio-temporal visualization of a set of DVS events in response to a rotating bar.

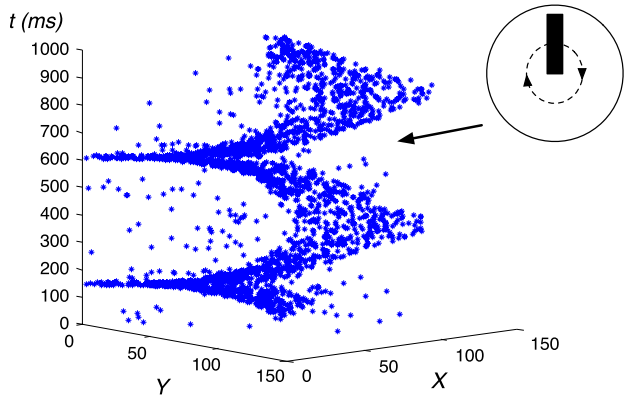

Fig. 1. Space–time representation of events generated in response to a rotating black bar. Each dot represents a DVS event.

2.3. Noise

Every pixel has a spontaneous impulse activity decorrelated from the content of the scene. With the retina used in this study, each pixel emits a noise impulse every 15 s with a standard deviation of 1.5 s. The primary source of spontaneous activity is a fixed time pattern noise, mainly due to the leaky switch that resets the pixel after the generation of a spike (Lichtsteiner et al., 2008). The variability of every pixel is highly unpredictable due to the mismatch in the silicon substrate. As spontaneous events are occurring randomly, experiments show that 92% of noise can be suppressed using a median filter or a contra harmonic mean filter, that is usually used to remove salt and pepper noise.

3. Event-based optical flow

The main assumption for the evaluation of the optical flow is the invariance of light intensity captured by the retina undergoing a small motion over an infinitesimally short duration. If we assume that the brightness of a small surface patch is not changed by motion, then expansion of the total derivative of brightness leads to Barron, Fleet, and Beauchemin (1994):

$$\begin{aligned}\frac{dI(x,y,t)}{dt} &= \frac{\partial I}{\partial x}\frac{\partial x}{\partial t} + \frac{\partial I}{\partial y}\frac{\partial y}{\partial t} + \frac{\partial I}{\partial t} \\ &= \begin{pmatrix}\frac{\partial I}{\partial x} & \frac{\partial I}{\partial y}\end{pmatrix}^t \begin{pmatrix}\frac{\partial x}{\partial t} \\ \frac{\partial y}{\partial t}\end{pmatrix} + \frac{\partial I}{\partial t} \\ &= \mathrm{grad}^t(I)\begin{pmatrix}v_x \\ v_y\end{pmatrix} + \frac{\partial I}{\partial t} = 0, \end{aligned} \tag{1}$$

where is I is the image containing gray levels. This equation is solved for the velocity vector $(v_x, v_y)^t$ but it is under-determined, since two variables must be estimated, given only one equation. One of the most popular techniques Lucas and Kanade (1981b) to overcome this problem is based on the assumption of local constant flow: $(v_x, v_y)^t$ is constant over the neighborhood of pixel $(x, y)^t$. If the neighborhood is a $n \times n$ window, $m = n^2$ optical flow equations can be written as

$$\begin{pmatrix}\mathrm{grad}^t(I(x_1, y_1)) \\ \vdots \\ \mathrm{grad}^t(I(x_m, y_m))\end{pmatrix}\begin{pmatrix}v_x \\ v_y\end{pmatrix} = \begin{pmatrix}-I_{t_1} \\ \vdots \\ -I_{t_m}\end{pmatrix}, \tag{2}$$

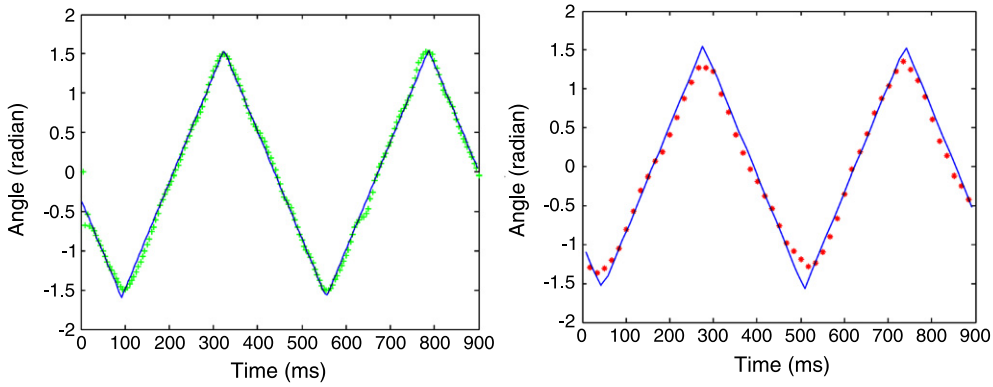

Fig. 2. Bar orientation estimated by the events-based (+) and by the frame-based (∗) optical flow algorithms versus the true bar orientation over the time (−) for the input shown in Fig. 1.

with gradt(I) being the spatial gradient and I_t the partial temporal derivative of I. The equation system can then be solved using least square error minimization techniques.

This constraint can be formulated in an event-based manner. The main difficulty being that event-based retinas do not provide gray levels. The absence of gray levels makes it difficult to provide a spatial gradient computation. Nevertheless for adjacent active pixels it is possible to provide an estimation of the spatial gradient by comparing their instantaneous activities:

$$\begin{cases} \dfrac{\partial e(x,y,t)}{\partial x} \sim \displaystyle\sum_{t-\Delta t}^{t} e(x,y,t) - \sum_{t-\Delta t}^{t} e(x-1,y,t) \\ \dfrac{\partial e(x,y,t)}{\partial y} \sim \displaystyle\sum_{t-\Delta t}^{t} e(x,y,t) - \sum_{t-\Delta t}^{t} e(x,y-1,t). \end{cases} \tag{3}$$

Δt is a temporal interval of few μs it is generally set to 50 μs. The estimation of the temporal gradient is expected to be more precise than in the frame-based framework due to the temporal precision of the DVS. It can be written as

$$\frac{\partial e(x,y,t)}{\partial t} \sim \frac{\displaystyle\sum_{t-\Delta t}^{t1} e(x,y,t) - \sum_{t-\Delta t}^{t} e(x,y,t)}{t - t_1}, \quad \text{with } t_1 < t. \tag{4}$$

By substituting Eqs. (3) and (4) into Eq. (2), the jth line of the matrix equality can be reformulated using events:

$$\begin{aligned} &\left(\sum_{t-\Delta t}^{t} e(x_j,y_j,t) - \sum_{t-\Delta t}^{t} e(x_j-1,y_j,t)\right) v_x \\ &+ \left(\sum_{t-\Delta t}^{t} e(x_j,y_j,t) - \sum_{t-\Delta t}^{t} e(x_j,y_j-1,t)\right) v_y \\ &= \frac{\displaystyle\sum_{t_1}^{t} e(x_j,y_j,t)}{t - t_1} \end{aligned} \tag{5}$$

since

$$\sum_{t-\Delta t}^{t1} e(x,y,t) - \sum_{t-\Delta t}^{t} e(x,y,t) = \sum_{t_1}^{t} e(x,y,t).$$

The general optic flow algorithm is detailed by *Algorithm* 1.

4. Experiments

Experiments use the DVS that has a temporal resolution of 1 μs. The optical flow is computed using a neighborhood of 5 × 5 pixels for a $\Delta t = 50$ μs.

Algorithm 1 Event-based optical flow

For each incoming e(x,y,t):
Define a $(n \times n \times \Delta t)$ neighborhood around $(x, y, t)^T$
Compute the partial derivatives:

- $\frac{\partial e(x,y,t)}{\partial x}$, $\frac{\partial e(x,y,t)}{\partial y}$, $\frac{\partial e(x,y,t)}{\partial t}$

Solve Eq. (2) written using Eq. (5) for $(v_x, v_y)^t$

4.1. Orientation

The first experiment uses a black bar painted on a white disk, rotating with a constant angular velocity of $\omega \sim 13.6$ rad/s. It is used as input to the DVS, as shown in Fig. 1. The events-based optical flow is computed in real-time using the continuous train of output events. The frame-based optical flow is computed for a 60 fps emulated camera, obtained by accumulating events for a duration of 16.7 ms. Fig. 2 shows the orientation of the bar computed from the flow obtained by the two techniques and is plotted versus the ground truth orientation of the bar. The event-based computation takes full advantage of the high temporal accuracy of the sensor, by providing a dense and accurate estimation of the rotation angles in real time.

4.2. Amplitude

The amplitudes of the estimated optical flow are computed for a moving pattern of bars presented on a moving conveyor belt whose translational speed can be accurately set by adjusting the supply voltage of a DC motor that drives the system (Fig. 3). In this experiment the magnitudes of the optical flow are computed for different known belt speeds obtained by driving the DC motor with supply voltages ranging from 500 to 1500 mV corresponding to a range of velocities of 30.83–83.05 cm/s. Fig. 3 shows the mean estimated amplitudes of the bars for a range of voltages, as expected, there is a linear relationship between the actual speeds and the velocity amplitudes.

4.3. Temporal precision

The experiment consists of the observation of a regular planar grid of LEDs with a precisely adjustable illumination frequency (see Fig. 4(a)). The panel has been designed so that each LED switches on and off sequentially and individually in time. The process starts from the first one located at the top left corner of the panel, and then proceeds progressively through every row until reaching the final LED in the bottom right-hand corner. The illumination sequence then commences again. The distance

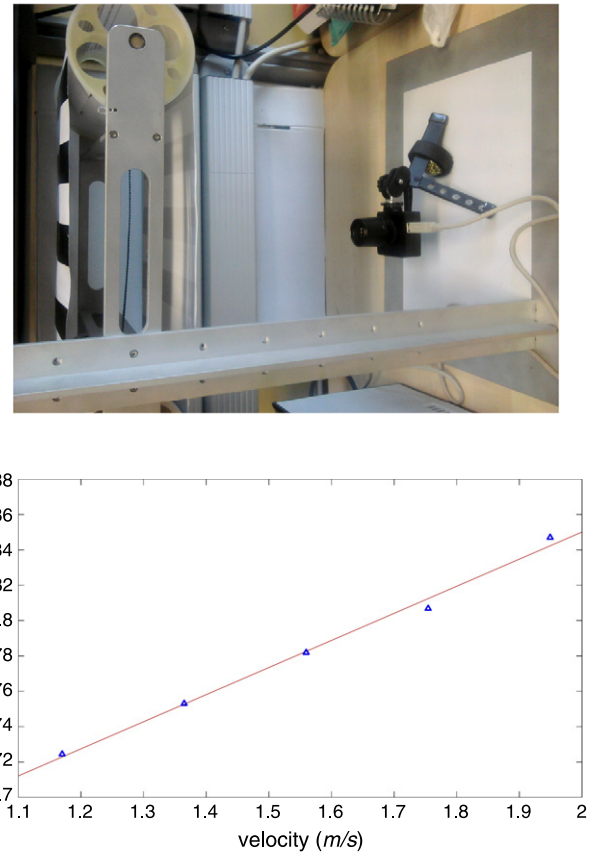

Fig. 3. (Top) Experimental device: a translating pattern of vertical bars on a belt moved by a DC is acquired by the DVS. (Bottom) Estimated amplitudes of the optical flow versus the DC voltage ranging from 500 to 1500 mV and corresponding to a range of velocities of 30.83–83.05 cm/s.

between LEDs is known to be 3.4 cm. The time interval between the switching of successive LEDs is adjustable from 1 ms to 1 s and is set to 16 ms in the current experiment.

The aim of the experiment is to estimate the rate of switching on of successive LEDs on the panel. The principle is to detect when two consecutive LEDs switch on. The speed can then be computed from the knowledge of this temporal interval, and the distance between successive LEDs. The switching on of an LED is detected by sensing the characteristic divergent pattern of the optical flow that it creates, as shown in Fig. 4(b). This divergent pattern of optical flow is created because, as the LED turns on, the pixel that views the brightest point in the LED reaches a threshold of activity first, followed later by the surrounding pixels.

In the experiment the DVS observes the panel continuously and for every incoming event the optical flow is computed. In a second stage, in order to detect precisely the exact timing of the LED's activation, a spatial vector pattern similar to Fig. 4(b) is used as a template and correlated with the measured optic flow pattern in the neighborhood of the active pixel's location. In the experiment, the vector flow pattern of activation is set to a size of 5×5 vectors.

Once the location of the active LED is located, its position on the panel is retrieved and the estimation of the speed of activation of pixels can then be performed. The precise moment of switching on of an LED is established by detecting the divergent pattern of optic flow that will initially cover a small area and then grow continuously. The instant of switching on is then defined as the time when the central pixel is first detected and has reached threshold. Fig. 4(c) shows the distribution of estimated speeds for a 2 s sequence, giving an estimated mean speed of 2.169 m/s while the ground truth speed is 2.125 m/s. The observed estimation errors are due to small misalignments of individual LEDs in the panel, small geometrical imperfections in the retina and distortions in the optics of the camera.

4.4. Computational cost

Tests were performed to compare the computational times required by the frame-based and the event-based methods for computing optic flow. These results were obtained using a C++ implementation of the algorithm, on an Intel Core 2 Duo 2.40 GHz processor.

The optical flow was computed for a rotating bar as shown in Fig. 1. The event-based method uses raw events, while the frame-based method uses frames acquired at a rate of 60 Hz created by summing events. The following computation times were obtained:

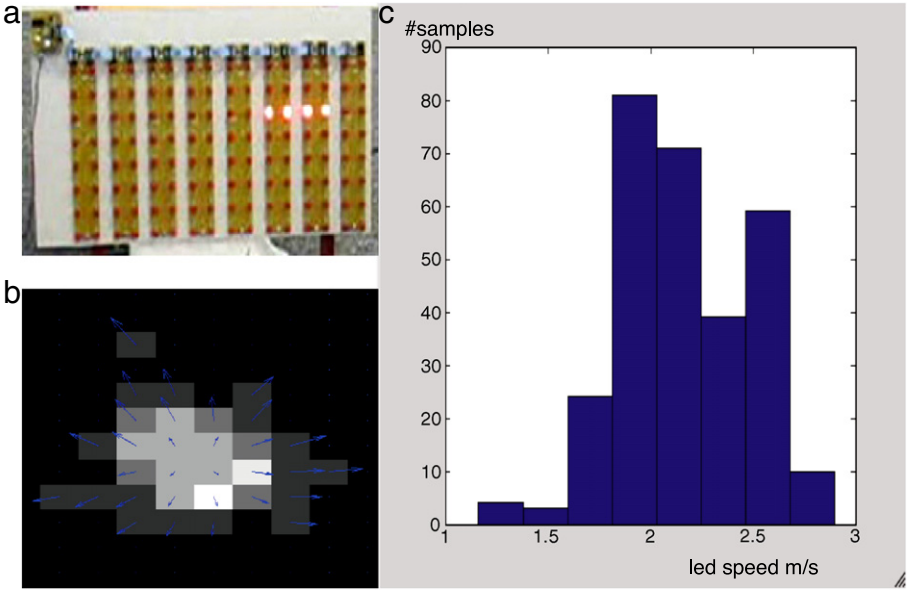

Fig. 4. Computation of the optical flow generated by sequential activation of LEDs on a panel. Long exposure of this image shows four LEDS that have been turned on successively from left to right (a). (b) Switching on of a single LED generates a characteristic, expansional pattern of optic flow. (c) Distribution of estimated speeds of moving display created by sequential switching of LEDs in m/s, giving a mean value of 2.16 m/s, compared to an actual speed of 2.12 m/s.

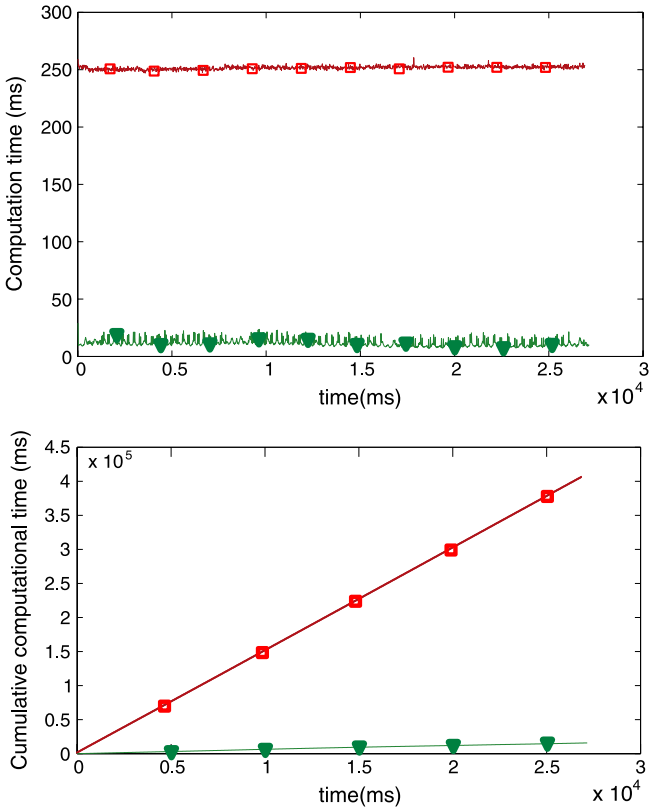

Fig. 5. Computation time of event-based (triangles) vs. frame based (squares) for the same observed sequence. The event-based method delivers flow measurements at a cost that is approximately 25 times lower than does the frame-based method.

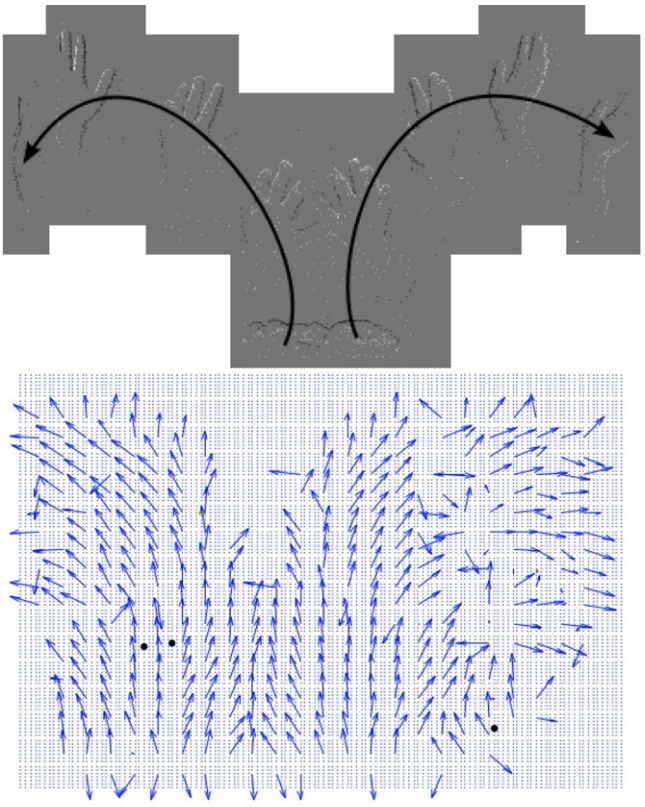

Fig. 6. Optic flow for curved motion: (up) decomposition of the movement of two hands moving from the bottom to the sides of the scene and its (down) corresponding cumulative estimated optic flow over a time period of 1.5 s on all the focal plane.

- frame-based, 60 fps (16.7 ms): the number of processed pixels at each step is 16 384, and a mean computation time is 251.7 ms,
- event-based (1e−3 ms): computation time for a period of 16.7 ms corresponding to a mean number of events of 1340, the computation time is 9.65 ms, while the mean computation time of an event is 7.2e−3 ms.

It takes 251.7 ms to compute the optical flow between two successive frames on a time interval between successive frames of 16.7 ms. This means that in the absence of any optimization, the optical flow can be computed only at a rate of 4 fps. The optical flow computation is taking as long as 251.7 ms because we are computing the flow at all of the 16 384 pixel locations in the imager without any optimization in both frame and event-based. The event-based optical flow requires 7.2 μs to compute the optical flow for each event, thus leading to a total time of $1340 \times (7.2e-3) = 9.65$ ms. Fig. 5 shows that the event-based method delivers flow measurements at a cost that is approximately 25 times lower than does the frame-based method.

4.5. Samples of computed flows

This section presents examples of optic flow computed using the events-based method developed in this paper. Fig. 6 presents the decomposition of fast arms movements and their corresponding estimated optical flows. Fig. 7 shows the optic flow associated with a bouncing ball.

5. Conclusions

This paper presented an alternative framework for the computation of optical flow based on an asynchronous spiking vision sensor that responds to temporal variations of contrast of the visual input. The experiments showed that asynchronous event-based acquisition allows for high dynamic, fast and low cost computation of the optical flow for many different stimuli.

The results presented here fully exploit the high temporal resolution and high dynamic range of event-based cameras, and outperform existing frame-based camera techniques, overcoming their limitations in relation to large displacements and limited accuracy in the calculation of the optical flow. The proposed paradigm should be valuable in a number of applications that require rapid, real-time analysis of high-speed events such as in imaging moving projectiles, or in vision-based guidance of high-speed autonomous aircraft.

Acknowledgments

The authors would like to thank T. Delbruck, R. Berner, P. Lichtsteiner, S.C. Liu and P. Rogister, for their help, time, availability and for allowing to use and share their knowledge in using AER cameras. This work was supported by the EU eMorph grant #ICT-231467, and partially by the Australian Research Council Centre of Excellence in Vision Science (CE0561903), by a Queensland Smart State Premier's Fellowship, and by US AOARD Award no. FA4869-07-1-0010.

The authors are also grateful to both the CapoCaccia and Telluride neuromorphic workshops for their important role in setting up the indispensable community gathering efforts at the core of this collaborative work.

Appendix. Supplementary data

Supplementary material related to this article can be found online at doi:10.1016/j.neunet.2011.11.001.

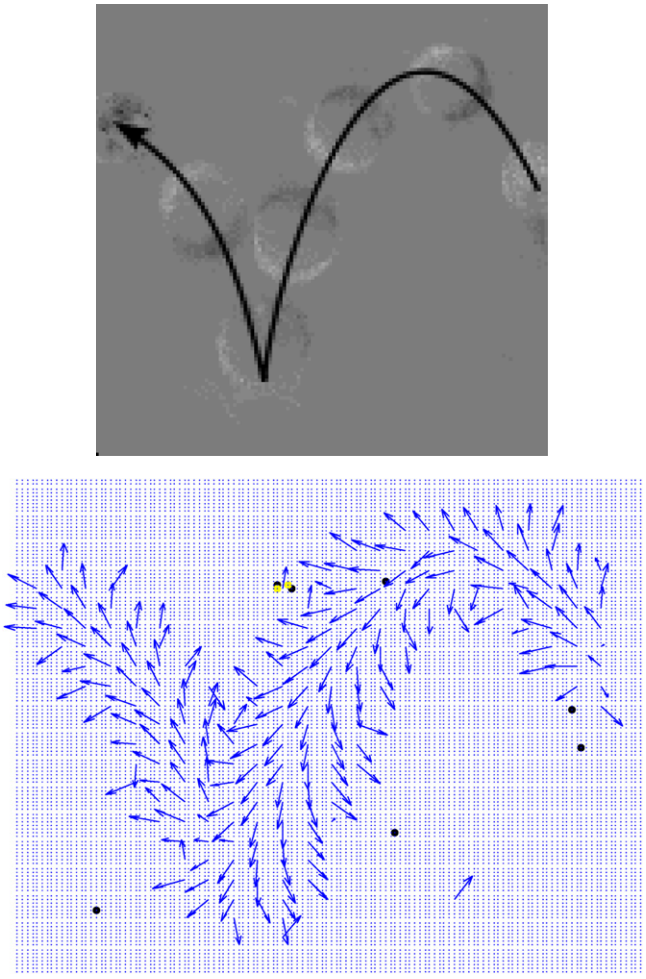

Fig. 7. Optic flow for curved motion: (up) decomposition of the movement of a bouncing ball, (down) corresponding cumulative estimated optic flow over a time period of 0.8 s on all the focal plane.

References

Alexander, S., Arteaga, G., David, J., & Tomas, W. (2008). A discrete search method for multi-modal non-rigid image registration. In *NORDIA 2008: proceedings of the 2008 IEEE CVPR workshop on non-rigid shape analysis and deformable image alignment* (pp. 6).

Amiaz, T., Lubetzky, E., & Kiryati, N. (2007). Coarse to over-fine optical flow estimation. *Pattern Recognition*, *40*, 2496–2503.

Barron, J., Fleet, D., & Beauchemin, S. (1994). Performance of optical flow techniques. *International Journal of Computer Vision*, *12*(1), 43–77.

Black, M., & Anandan, P. (1996). The robust estimation of multiple motions: parametric and piecewise-smooth flow fields. *Computer Vision and Image Understanding, CVIU*, 75–104.

Boahen, K. (2005). Neuromorphic microchips. *Scientific American*, *292*, 55–63.

Braddick, O. (2001). *Neural basis of visual perception*: *Vol. 0*. Elsevier Ltd., pp. 16269–16274.

Brox, T., Bruhn, A., Papenberg, N., & Weickert, J. (2004). High accuracy optical flow estimation based on a theory for warping. In *LNCS*: *Vol. 3024. European conference on computer vision*, ECCV, (pp. 25–36). Prague, Czech Republic: Springer.

Chicca, E., Lichtsteiner, P., Delbruck, T., Indiveri, G., & Douglas, R. (2006). Modeling orientation selectivity using a neuromorphic multichip system. In *Proc. IEEE int. symp. circuits syst.* Press (pp. 1235–1238).

Choi, T. Y. W., Merolla, P., Arthur, J., Boahen, K., & Shi, B. E. (2005). Neuromorphic implementation of orientation hypercolumns. *IEEE Transactions on Circuits and Systems*, *52*, 1049–1060.

Fransens, R., Strecha, C., & Gool, L. V. (2007). Optical flow based super-resolution: a probabilistic approach. *Computer Vision and Image Understanding, CVIU*, *106*(1), 106–115.

Horn, B., & Schunck, B. (1980). Determining optical flow. *Tech. Rep*. Cambridge, MA, USA.

Lenero-Bardallo, J. A., Serrano-Gotarredona, T., & Linares-Barranco, B. (2011). A 3.6us asynchronous frame-free event-driven dynamic-vision-sensor. *IEEE Journal of Solid-State Circuits*, *46*, 1443–1455.

Lichtsteiner, P., Posch, C., & Delbruck, T. (2008). A 128 128 120 dB 15 s latency asynchronous temporal contrast vision sensor. *IEEE Journal of Solid-State Circuits*, *43*(2), 566–576. doi:10.1109/JSSC.2007.914337.

Liu, H., Hong, T., Herman, M., Camus, T., & Chellappa, R. (1998). Accuracy vs. efficiency trade-offs in optical flow algorithms. *Computer Vision and Image Understanding*, *72*(3), 271–286.

Lucas, B., & Kanade, T. (1981a). An iterative image registration technique with an application to stereo vision (IJCAI). in: *Proceedings of the 7th international joint conference on artificial intelligence. IJCAI'81* (pp. 674–679).

Lucas, B., & Kanade, T. (1981b). An iterative image registration technique with an application to stereo vision. In *Imaging understanding workshop* (pp. 121–120).

Mahowald, M., & Mead, C. (1991). The silicon retina. *Scientific American,*.

Mead, C. (1989). Adaptive retina. In C. Mead, & M. Ismail (Eds.), *Analog VLSI implementation of neural systems*.

Memin, E., & Perez, P. (1998). Joint estimation-segmentation of optic flow. In *ECCV'98*.

Posch, C. (2010). High-DR frame-free PWM imaging with asynchronous aer intensity encoding and focal-plane temporal redundancy suppression, in: ISCAS.

Posch, C., Matolin, D., & Wohlgenannt, R. (2011). A QVGA 143 dB dynamic range frame-free PWM image sensor with lossless pixel-level video compression and time-domain CDS. *IEEE Journal of Solid-State Circuits*, *46*, 259–275.

Roska, B., Alyosha, M., & Werblin, F. (2006). Parallel processing in retinal ganglion cells: how integration of space–time patterns of excitation and inhibition form the spiking output. *Journal of Neurophysiology*, *95*(6), 3810–3822. arXiv:http://jn.physiology.org/cgi/reprint/95/6/3810.pdf, doi:10.1152/jn.00113.2006, URL: http://jn.physiology.org/cgi/content/abstract/95/6/3810.

Serrano-Gotarredona, R., Oster, M., Lichtsteiner, P., Linares-Barranco, A., Paz-Vicente, R., & Gomez-Rodriguez, F. (2009). Caviar: a 45k-neuron, 5m-synapse, 12g-connects/sec aer hardware sensory-processing-learning-actuating system for high speed visual object recognition and tracking. *IEEE Transactions on Neural Networks*, *20*, 1417–1438.

Serrano-Gotarredona, R., Serrano-Gotarredona, T., Acosta-Jimenez, A., & Linares-Barranco, B. (2006). A neuromorphic cortical-layer microchip for spike-based event processing vision systems. *IEEE Transactions on Circuits and System*, *53*, 2548–2566.